Electron tunneling spectroscopy on superconducting Al-doped MgB_2 thin films: π energy gap and Eliashberg function

R. Schneider,[1,*] A. G. Zaitsev,[1] O. De la Peña-Seaman,[1,2] R. de Coss,[2] R. Heid,[1] K.-P. Bohnen,[1] and J. Geerk[1]
[1]*Institute for Solid-State Physics, Karlsruhe Institute of Technology, Campus North, P.O. Box 3640, D-76021 Karlsruhe, Germany*
[2]*Departamento de Física Aplicada, Centro de Investigación y de Estudios Avanzados del IPN, Apartado Postal 73, Cordemex 97310 Mérida, Yucatán, Mexico*

(Received 18 November 2009; revised manuscript received 28 January 2010; published 24 February 2010)

Superconducting thin films of composition $Mg_{1-x}Al_xB_2$ with $0 \leq x < 0.5$ were prepared *in situ* by sublimation of Mg combined with B and Al magnetron sputtering. The critical temperature T_c decreased linearly with x up to 0.4. For $0.4 < x < 0.5$ the formation of a plateaulike feature at a $T_c \approx 12$ K was observed. This effect is supposed to be due to the incipient formation of the superstructure $MgAlB_4$ with ordered alternating Mg and Al planes separated by B planes. To detailedly study the influence of Al doping on the electron-phonon coupling in the polycrystalline films with a preferred c-axis texture quasiparticle tunneling experiments were performed on planar tunnel junctions with natural thermal oxide or artificial aluminum oxide tunnel barriers. Differential conductance measurements at low-bias voltage and low temperature of superconductor-insulator-superconductor tunnel junctions allowed the direct determination of the energy gap of the Fermi surface π sheet. The π energy gap decreased linearly with decreasing T_c of the films in agreement with the model of band filling. Whereas all the tunneling studies published so far mainly revealed features of the two energy gaps, the observation of phonon-induced structures in the differential conductance measurements at high bias voltage, i.e., in the phonon region, in this study enabled the important determination of the energy-dependent Eliashberg function α^2F of the Fermi surface π sheet for various Al doping levels. Compared to the undoped MgB_2, significant changes in α^2F could be observed that were confirmed by first-principles calculations.

DOI: 10.1103/PhysRevB.81.054519 PACS number(s): 74.50.+r, 74.70.Ad, 74.62.Bf

I. INTRODUCTION

The surprising discovery of superconductivity at $T_c = 39$ K in the long known[1] simple binary compound MgB_2 by Nagamatsu *et al.*[2] triggered great efforts in both basic and applied research. However, the hope of finding other superconductors in the material class of the diborides with even higher T_c was not fulfilled: The related isostructural stoichiometric compounds, for instance, AlB_2, NbB_2, TaB_2, and ZrB_2, do not superconduct.[3,4] Among the diborides MgB_2 seems to be an isolated sample of a superconductor with an exceptionally high T_c in contrast to the recently synthesized iron pnictides[5] among them many superconductors derived from a nonsuperconducting parent compound exist.[6]

Beside the quest for superconductivity in compounds of the same chemical family, chemical doping or alloying is a promising method to tune superconducting properties like T_c, the critical current density j_c in a magnetic field, and the upper critical field H_{c2}. Prominent representatives are, e.g., Nb-Ti,[7] doped La_2CuO_4,[8] and $BaFe_2As_2$.[9] Doping of MgB_2, however, has proven to be a difficult task. Merely a few cases of partial substitution of Mg or B have been substantiated, namely, Al, Mn, and Sc substitution of Mg and C substitution of B.[10] The most attention has been paid to C and Al doping.

The solid solution $Mg_{1-x}Al_xB_2$ exists across the whole series $0 \leq x \leq 1$ from MgB_2 to AlB_2 and is superconducting up to $x \approx 0.5$. T_c decreases with increasing Al doping level x.[11] Specimens have been prepared so far in the form of single crystals[12] and polycrystalline bulk.[13] To our knowledge, thin films have not been grown up to now. With respect to the structural properties, the a and c-axis lattice parameters of the hexagonal unit cell decrease with increasing Al content, and a possible "two phase region" may exist between $x=0.1$ and 0.25[11] which was, however, not confirmed in a subsequent study.[14] There are also significant changes in the electronic structure: Al doping of the two-band two-gap superconductor MgB_2 provides extra electrons that fill holes in the electronic σ bands, according to band-structure calculations.[15,16] Thereby, the electronic density of states at the Fermi energy, N(0), is reduced, and the electron-phonon coupling, that is directly proportional to N(0), decreases. This band filling model can explain the successive loss of superconductivity in the solid solution with increasing Al content x.[17] When the bands are completely filled, which takes place at $x \approx 0.56$, superconductivity disappears in fair agreement with experimental findings. At this critical concentration, the σ part of the Fermi surface has vanished. The collapse of the cylindrical σ sheets of MgB_2 through Al doping progresses gradually due to the decreasing radius of the cylinders. At $x \approx 0.27$ an electronic topological transition occurs and they take shape of a sandglass. For larger x the sandglass breaks into two separated cones.[17,18]

The evolution of the two superconducting energy gaps Δ_σ (the large gap) and Δ_π (the small gap) for Al and C doping of MgB_2 has been described by two theoretical models: the above mentioned band filling model[15–19] and the interband impurity scattering model.[20–23] Both models predict a T_c reduction and a decrease of the large gap Δ_σ with increasing doping level. However, for the small gap Δ_π the predictions are diametrically opposite: Band filling lowers Δ_π whereas interband scattering by impurities increases Δ_π so that a merging of the two gaps is expected. If both effects are si-

multaneously active, they can compensate and a constant Δ_π is expected with doping.

The dependence of both energy gaps on T_c, i.e., doping level, has been measured by means of various techniques in different Al doped MgB_2 samples: specific heat of polycrystals,[14] point contact spectroscopy (PCS) and point contact Andreev reflection (PCAR) on single and polycrystals,[24–26] and scanning tunneling spectroscopy (STS) on single crystals.[27] Polycrystals and thin films of undoped MgB_2 damaged with neutron irradiation have also been studied by specific heat measurements and STS.[28,29] Furthermore, the effect of disorder in MgB_2 thin films grown by different techniques on the energy gaps was investigated using STS.[30] For the large gap the experimental results are very clear, there is no doubt that Δ_σ decreases monotonically with decreasing T_c although the gap values scatter over a wide range depending on measurement method and specific sample. The measurements of the small energy gap, however, do not result in a uniform picture. On the one hand, Δ_π appears to be nearly constant or slightly increasing for low-doping levels up to 10% Al and decreasing for higher doping as suggested by specific heat, point contact and scanning tunneling measurements on single and polycrystals.[14,24,25,27] On the other hand, specific heat and point contact data indicate a monotonic decrease in Δ_π with decreasing T_c.[26,31,32] Moreover, in radiation damaged and disordered MgB_2 thin films monotonically increasing or weakly affected values of Δ_π were found by scanning tunneling measurements.[29,30] Corresponding results on C-doped samples are not less controversial.[33] The striking disagreement might be due to differences in the determination of the doping level, an inhomogeneous distribution of the dopant within the crystal lattice, different methods of T_c measurements and the determination of the gap values. The above mentioned thermodynamic and spectroscopic methods use a considerable number of fitting parameters including the gap values themselves to evaluate the experimental raw data.

In this paper we report on the *in situ* preparation of Al doped MgB_2 thin films with composition $Mg_{1-x}Al_xB_2$ ($0 \le x < 0.5$). The dependence of T_c of the films on the Al concentration x was studied and compared with investigations on single and polycrystalline bulk samples published in the literature and theoretical predictions based on Eliashberg theory. The main purpose of the thin film activity was the preparation of planar sandwich-type crossed-strip tunnel junctions for electron tunneling. This type of junctions was described and extensively studied by Giaever[34] and McMillan and Rowell.[35] The high quality of the junctions enabled precise measurements of current (I)-voltage (V) characteristics and their first and second derivatives dI/dV and d^2I/dV^2, respectively, up to high dc bias voltage of 120 mV. Accurate values of the small energy gap Δ_π were obtained by use of superconductor (S)–insulator (I)–superconductor (S′) junctions at low temperature without the need of any fitting parameters. Fingerprints of the large gap, however, could not be observed among the large number of junctions under investigation. By measuring the local T_c of the film at the position of the small junction, the so-called gap T_c, where the closing of the energy gap with increasing temperature is observed, an approximately linear Δ_π versus T_c relation was found and compared with experimental and theoretical data available in the literature. In the range of the phonons, between 30 and 120 mV, phonon-induced changes in the differential conductance of S-I-normalconductor N junctions could be detected. They were used to determine effective Eliashberg functions for various Al concentrations by the solution of the single-band Eliashberg equations with the proximity version of the McMillan-Rowell computer code. The effective Eliashberg functions with the Al doping level as a parameter and their comparison with first principles calculations allowed to follow the progressive loss of superconductivity accompanied by the gradual decrease of the interband pairing interaction and the strong hardening of the optical phonons at the high-energy end of the spectrum.

TABLE I. Residual gas pressure p_{res}, substrate temperature T_S, evaporator temperature T_E, Ar partial pressure p_{Ar}, B rf power P_B, and Al dc power P_{Al} for the synthesis of $Mg_{1-x}Al_xB_2$ thin films with $0 \le x < 0.5$.

p_{res} (mbar)	T_S (°C)	T_E (°C)	p_{Ar} (mbar)	P_B (W)	P_{Al} (W)
2×10^{-8}	420–460	500–520	2.1×10^{-2}	600–700	0–350

II. THIN FILMS AND JUNCTIONS

The $Mg_{1-x}Al_xB_2$ ($0 \le x < 0.5$) thin films with a thickness of 300 nm were deposited onto 20×10 mm^2 sized r-plane and c-plane sapphire substrates. The deposition system and the *in situ* deposition process were comprehensively discussed in Refs. 36–38 for pure MgB_2 thin films. Only minor changes had to be made for Al doping. Briefly, small pieces of Mg were sublimated in a cylindrical oven surrounding a substrate heater to provide a high-Mg vapor pressure at the position of the heated substrate. B was radio-frequency (rf) magnetron sputtered from a planar sintered target above the oven. Al as a dopant was dc magnetron sputtered from a planar metallic target next to the oven. The deposition parameters are summarized in Table I. At substrate temperatures T_s between 420 and 460 °C the films grew in columnar grains that were crystallographically textured with the c-axis perpendicular to the substrate surface. The level of doping with Al was controlled by adjusting the Al sputtering power P_{Al} that was kept constant over the entire deposition time of 30 min. In the applied power range from 0 to 350 W the doping parameter x proved to be directly proportional to P_{Al} with the empirical relationship $x = 1.5 \times 10^{-3}$ W$^{-1} \times P_{Al}$(W).

The composition of the films, in particular the Mg/Al ratio, was determined by Rutherford backscattering spectrometry (RBS) using 2 MeV $^4He^+$ particles.[39] Since the analytical beam hit the thin film in an area of about 1 mm^2, the spectrum of the backscattered particles yielded information on the overall composition of a small sample volume. To test the compositional homogeneity over the whole film area the beam was directed to three different positions on the rectangular sample, namely, the middle and the upper and lower edges. The deviations from the averaged Al amount x were not larger than ± 0.02 for the various positions so that the

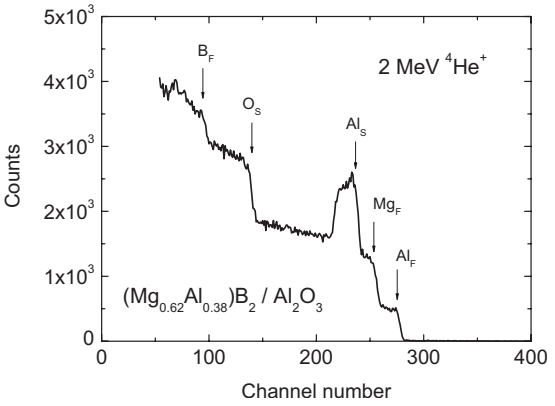

FIG. 1. Exemplary RBS spectrum of an Al doped MgB_2 thin film on *r*-plane sapphire substrate. Such spectra were used to determine the Al doping level x, here $x=0.38\pm0.02$ (F=film, S=substrate).

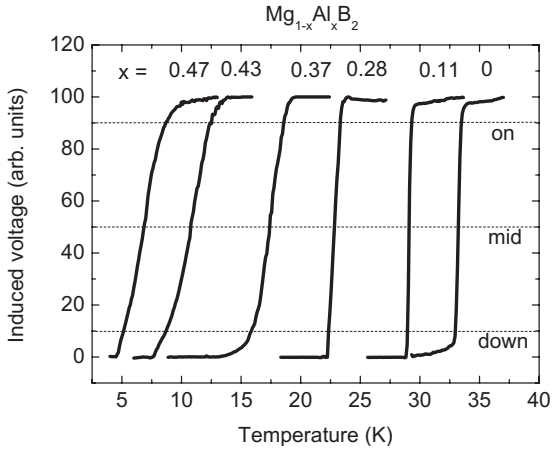

FIG. 2. Set of inductively measured superconductive transitions with the Al doping level x as a parameter. The transition curves are described by the characteristic temperatures onset, midpoint, and downset (see dashed horizontal lines).

films were laterally quite homogeneous in composition. The maximum relative error $(\Delta x/x)_{max}$ of the average x was estimated to be 10% $(1-x)$. The RBS spectrum of an Al doped MgB_2 thin film on *r*-plane sapphire substrate with $x=0.38\pm0.02$ is shown in Fig. 1. The $^{27}Al_F$ and $^{24}Mg_F$ (F=film) element edges are well separated. Because of the missing O_F edge between the O_S and Al_S (S=substrate) edges (cf. Figure 3 of Ref. 37), contamination with oxygen in this sample is below the resolution limit of roughly one atomic percent. The preparation of the films without incorporation of oxygen is almost impossible due to the strong oxygen affinity of the constituents and the finite residual gas pressure. In our experience there is generally a slight oxygen contamination of a few atomic percent.

T_c of the films was measured by means of a contactless inductive method where the voltage signal induced by a small alternating magnetic field breaks down upon entering the superconducting state due to the shielding effect. Since persistent current loops of large extension are necessary for shielding, the inductive method samples a larger volume of the film for superconductivity than the resistive method where a continuous linear path of superconducting material is enough for shortening the voltage contacts. In this sense the applied inductive method is sensitive to superconductivity in the volume of the thin film. A series of six inductively measured transitions to superconductivity is illustrated in Fig. 2 with the Al doping level x as a parameter. The transition curves can be described by three characteristic temperatures: onset (90% of the full voltage signal), midpoint (50%), and downset (10%). The difference between onset and downset is defined as the transition width ΔT_c. The midpoint, referred to as the T_c, of the pure MgB_2 film ($x=0$) only amounts to 33.2 K and is considerably smaller than the bulk T_c of 39 K. T_c of our MgB_2 films showed a monotonically increasing dependence on the substrate temperature T_s (cf. Figure 1 of Ref. 38) and we had to apply a T_s of 550 °C to reach a T_c of 37 K close to the bulk value. In this study we intentionally deposited the films at significantly lower T_s of 420 to 460 °C (Table I) for two reasons, the discharge of the B sputter gun was much more time stable and the films for our tunnel junctions in Ref. 40 also had T_c values between 32 and 34 K. Those junctions are the references which we have to compare the tunnel junctions of the present study with. Figure 2 demonstrates the rapid decrease in T_c down to 6.8 K for x increasing up to 0.47 ± 0.03. The transition widths ΔT_c of 0.3 to 1 K remain small for $x<0.3$. Above this value a sudden increase of ΔT_c is observed up to 4 K at x around 0.5. This feature is discussed later in the context of the T_c versus x relationship.

Tunneling using crossed-strip junctions is comprehensively described in Ref. 35. In this study a freshly deposited $Mg_{1-x}Al_xB_2$ film served as the base electrode on the sapphire substrate. The insulating tunnel barrier was either a native oxide layer of the film or an artificial overlayer of after-oxidized Al metal[41] that was deposited on the boride film by means of dc magnetron sputtering without breaking the vacuum. In order to get junctions with the appropriate tunneling resistance between 10 and 10^4 Ω, which is the best range for the electrical measurements, the artificial overlayer or the native oxide layer had to be employed for films with Al contents $x<0.4$ and $x>0.4$, respectively. Since the performance of both types of junctions was quite similar, it can be concluded that the native oxide on an Al-rich film resembles a thin oxidized Al layer, e.g., due to Al segregation at the film surface. The native oxide was grown by cooling down the films in 2.1×10^{-2} mbar Ar to 50 to 60 °C after deposition and by exposing them to a flow of pure oxygen that filled the preparation chamber to the ambient pressure of one atmosphere within 90 s. Pure oxygen was chosen to avoid contamination or chemical reaction of the oxide with molecules like CO_2 or H_2O. It is well known that layers of organic molecules can drastically change the barrier properties.[42] For the artificial overlayer, the Al film was deposited at a substrate temperature of 170 °C with a nominal thickness of 0.9, 1.8, or 3.6 nm. The oxidation procedure was the same as described above for the formation of the native oxide on the Al-rich films. It is worth mentioning that deposition of the Al film at room temperature resulted in short circuit junctions. Hence, we conclude that the Al overlayer incompletely wets the underlying Al doped MgB_2 film at

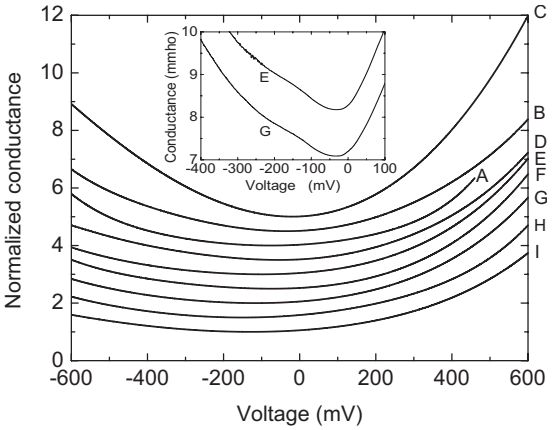

FIG. 3. Normalized conductance after elimination of the inelastic tunneling contribution versus bias voltage for various junctions A to I. Each characteristic is normalized to its minimum value. The characteristics are shifted in vertical direction for clarity. The inset shows the conductance increase due to inelastic tunneling for junctions E and G. The voltage polarity is that of the In counterelectrode. A, B, and C: Junctions with native oxide barrier. D to I: Junctions with artificial Al_2O_3 overlayer.

room temperature. The crossed-strip In counterelectrode was evaporated through a shadow mask. Indium was chosen because of its low-critical field of 38 mT at 0 K so that a small magnetic field of 100 mT was sufficient to fully suppress superconductivity in the counterelectrode when phonon-induced structures were measured on superconductor-insulator-normalconductor (SIN) junctions. The junction area was in the order of magnitude 0.1 mm^2, and the tunneling resistance ranged from a few tens of ohms to a few kiloohms for the native oxide barrier and the artificial overlayer, respectively. A four-probe arrangement with separate current and voltage leads was used for performing the electrical measurements.

The formation of the tunnel barrier is a bottleneck of junction preparation. Its properties can be deduced from normal-state tunneling characteristics, even quantitatively in a simplicative manner. Therefore, differential conductance measurements, dI/dV, with the electrodes in the normal state over a wide range of bias voltage V were used to determine the properties of the barrier oxide. The inset of Fig. 3 shows the conductance of two junctions E and G as measured from −0.4 to 0.1 V. Both characteristics reveal a sudden conductance increase of 2 to 4% at around −120 mV which is believed to be due to an inelastic tunneling effect. In the junctions E and G this effect was not resolvable for positive bias because of the stronger increase of the overall conductance compared to negative bias. In order to obtain the elastic tunneling conductance, which directly reflects the properties of the barrier, the inelastic contribution was eliminated as described in Ref. 36. The normalized conductance of the elastic tunneling channel against the bias voltage from −0.6 to 0.6 V is shown in the main part of Fig. 3 for $Mg_{1-x}Al_xB_2$-insulator-In junctions with $x=0$ (junction A), $x=0.08$ (junctions B and C), and $x=0.12$ (junctions D to I). The measurements were carried out at temperatures between 28 and 35 K with both electrodes in the normal state. For all the junctions the minimum conductance, which is offset from zero bias toward negative bias, was normalized to one, and the curves were shifted in the vertical direction for clarity. The traces A to I reflect the voltage dependence of the tunneling matrix element T following the theory of electron tunneling:[43] $(dI/dV)_{NN'} \propto N_1(0)N_2(0)|T|^2$, where $N_1(0)$, $N_2(0)$ are the densities of states at the Fermi energy of the base and the counterelectrode, respectively. In tunneling spectroscopy, a figure of merit for conductance curves such as those in Fig. 3 is their flatness, since the tiny phonon induced features in SIN junctions that will be discussed later, are superposed on this background and can obviously be better resolved when it is flat, i.e., only slowly varying with voltage. The shape of the background is correlated with the thickness and height of the tunnel barrier: A steep background reflects a thick and shallow barrier, whereas the aimed flat one indicates a thin and high barrier. At first glance the curves A to I are all flatter for negative bias with the conductance minima offset from zero to negative bias reflecting an asymmetry of the tunnel barrier. Curve A was measured on a junction with pure MgB_2 ($x=0$) base electrode and a native oxide layer grown at 160 °C as a tunnel barrier (cf. Ref. 36). Starting from the minimum the conductance increases by a factor of 2.2 over a bias range of 450 mV on the left horizontal scale. The conductance characteristics of junctions with $Mg_{0.92}Al_{0.08}B_2$ and natural oxide layers grown at 160 °C and 80 °C are represented by traces B and C, respectively. While B is quite similar to A, curve C is much steeper, and the conductance increases by a factor of 3.5 over 450 mV to the left starting at the minimum. With the same oxidation temperature of 160 °C a small Al amount does not seem to change much the barrier properties. However, a lower oxidation temperature of 80 °C obviously results in thicker and lower barriers. A significant progress in the properties of barriers on films with an Al content $x<0.4$ was reached by employing the Al overlayer technique as evidenced by the flatness of traces D to I: The increase of the conductance with factors from 1.6 to 1.8 is much smaller than that of junctions A, B, and C suggesting thinner and higher potential barriers. The uniformity of the set of junctions D to I demonstrates the high reproducibility and reliability of the Al overlayer technique. Applying the trapezoidal potential barrier model developed by Simmons and Rowell[44] and Brinkman[42] we were able to roughly estimate the thickness s and the average height φ of the barrier. As already expected from the above estimates of the flatness of the conductance characteristics the thickness of the native oxide barriers increases from 1.6 to 1.9 nm and the height decreases from 1.6 to 1.0 eV for junctions A, B, and C, respectively. For the Al overlayer junctions we obtained $s=1.4$ nm and $\varphi=2.4$ eV. Both values are close to the values reported in the literature for Al_2O_3 tunnel barriers.[41,45]

All our junctions prepared on Al doped MgB_2 films exhibited a proximity effect[46] due to the unintended presence of a normalconducting thin layer between the diboride superconductor and the tunnel barrier. The effect showed up in the reduced density of states or RDOS (see Fig. 10) by a shift of the data points to negative values, particularly strong at low energy close to the energy gap. In this case, a sum rule for the RDOS,[47] that is immediately derived from the conserva-

tion of the particle number, when going from the normal- to the superconducting state, results in negative values, because a part of the states below the energy gap are occupied.[46] Other manifestations of the proximity effect like the typical "knee" structure in the *I-V* characteristic that causes a dip in the dI/dV characteristic just above the sum of the gaps in SIS′ proximity junctions were not observed in our junctions, probably because the energy gap of the In counterelectrode was too small for resolving those features or because the proximity layer between the superconducting boride film and the Al_2O_3 tunnel barrier was ultrathin or strongly coupled to the superconductor.[48] Since junctions on undoped MgB_2 films with native oxide layers were proximity free, the conjecture is obvious, that Al as a dopant or a constituent of the barrier is the key to the nature of the proximity layer. It might consist of Al segregated at the surface of the $Mg_{1-x}Al_xB_2$ film or of a few layers of Al-rich degraded $Mg_{1-x}Al_xB_2$, and even a contribution of the Al oxide to the proximity layer cannot be ruled out. The deformation of the RDOS caused by the proximity effect has an implication on the determination of the Eliashberg function α^2F by using the McMillan-Rowell (MMR) procedure for the inversion of the Eliashberg equations. Without proximity effect, the inversion is mostly performed with the standard MMR-computer code as described by Hubin in Ref. 49. To enable the inversion for proximity tunnel junctions, two "proximity parameters" had to be introduced allowing a proximity McMillan-Rowell (PMMR)-inversion analysis.[50] The two parameters are an elastic scattering strength d/l and $R=2d/\hbar v_F^*$, where d is the thickness of the proximity layer, l the effective scattering length or mean free path, and v_F^* the renormalized Fermi velocity in the proximity layer. The exponential term $\exp(-2d/l)$, which is responsible for the above mentioned reduction of the RDOS, and the cosine term cos(2RE) in the expansion of the tunneling density of states in the high-energy limit represent the scattering responsible for the above mentioned violation of a sum rule and the phase shift of quasiparticles within the proximity layer, respectively. In the PMMR program, both quantities d/l and R are entered as independent fitting parameters and varied until the best fit between the calculated and the experimental RDOS is reached.

In order to determine the quasiparticle density of states and the energy gap of the superconducting $Mg_{1-x}Al_xB_2$ thin films, measurements of the differential conductance dI/dV have been performed at low-dc bias voltage. To this end a standard ac modulation technique with phase sensitive harmonic detection and a constant-voltage source after Blackford were used.[51] The phonon-induced structure in the tunneling density of states was studied by measuring the differential resistance dV/dI and its derivative d^2V/dI^2 at high voltage. These measurements were carried out with the standard ac modulation and constant-current harmonic detection technique in combination with a high-resolution bridge circuit.[52] The differential resistance and its derivative can be converted into the differential conductance and its derivative by the following equations: $dI/dV=1/(dV/dI)$ and $-d^2I/dV^2=(d^2V/dI^2)/(dV/dI)^3$.

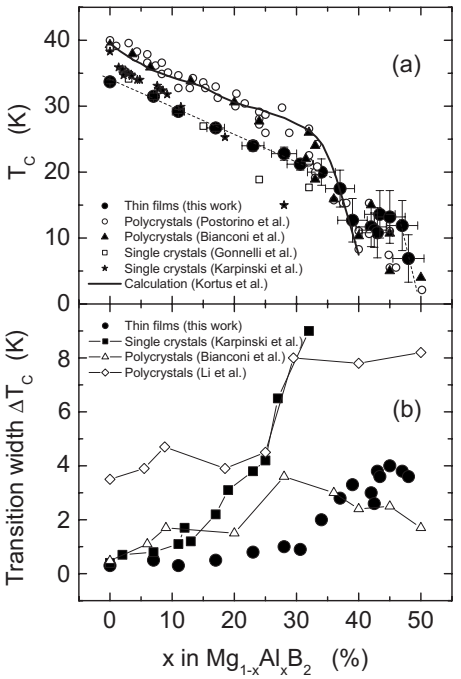

FIG. 4. (a) Transition temperature T_c of $Mg_{1-x}Al_xB_2$ thin films (●, this work), polycrystals (○, Ref. 13, and ▲, Ref. 53) and single crystals (□, Ref. 54, and ★, Ref. 12) in dependence on the Al concentration x. The straight line is the result of a calculation by Kortus *et al.*, Ref. 19. The dashed lines are guides to the eye. The horizontal and vertical bars indicate the absolute error $\pm\Delta x$ and the transition widths ΔT_c, respectively. (b) Transition width ΔT_c of $Mg_{1-x}Al_xB_2$ thin films (●, this work), single crystals (■, Ref. 12), and polycrystals (△, Ref. 53, and ◇, Ref. 55) versus x.

III. RESULTS AND DISCUSSION

A. T_c of $Mg_{1-x}Al_xB_2$ thin films versus x

Figure 4(a) shows our inductively measured $T_c(x)$ data that can be divided into four sections. In the first section ($0\leq x\leq 0.34$) T_c decreases almost linearly from the starting value of 33.8 K for $x=0$ with a slope of −0.4 K per atomic percent Al. The starting T_c of the pure MgB_2 films is lower than the bulk T_c for the reasons stated above. In the second section, between 0.34 and 0.39, a sudden steepening of the T_c drop occurs. The third section ($0.39\leq x\leq 0.47$) is characterized by a fluctuation of the T_c values between 11 and 14 K that suggests a plateaulike behavior. In the fourth section, T_c continues to decrease to zero at around 0.50. For comparison, $T_c(x)$ data measured by other groups on polycrystals and single crystals are included in Fig. 4(a). Apart from the difference in the absolute values of T_c the data for the polycrystals reproduce the linear decrease followed by the steepening quite well. The T_c values of the single crystals up to $x=0.32$ do not reveal such a clear linear dependence. A plateaulike behavior in the presented data for polycrystals can hardly be recognized, however, it is reported in Ref. 55. The straight line in Fig. 4(a) was obtained from the solution of the two-band Eliashberg equations taking into account the effect of band filling on the electronic density of states and the renormalization of the phonon frequencies, but not including interband impurity scattering.[19] It is evident that the

assumption of band filling is sufficient to explain the observed T_c decrease. The behavior of ΔT_c is illustrated in Fig. 4(b) where our results on thin films are contrasted with transition widths of single and polycrystalline bulk samples of other groups.[12,53,55] Up to $x=0.3$ the thin films show the smallest transition widths, and between 0.3 and 0.5 the values are comparable with those of polycrystals by Bianconi *et al.*[53] whereas the single and polycrystal values by Karpinski *et al.*[12] and Li *et al.*,[55] respectively, are significantly larger over the whole range of x. If the superconductive transition width is considered as a measure of the homogeneity of the Al distribution within the specimen, the films are highly homogeneous at least for $x<0.3$. This finding is in accordance with the results of the RBS measurements mentioned above that revealed high lateral homogeneity in the film composition. Interestingly each of the data sets shows a sudden, more or less pronounced increase of ΔT_c between approximately 20 and 30 percent Al. The increasing broadening of the transition accompanied by the sharp drop of T_c seem to be associated with the topological change of the σ part of the Fermi surface from cylinders via sandglass to separated cones as predicted by band-structure calculations for $x\approx 0.3$.[17,18,22,53] The observed $T_c(x)$ and $\Delta T_c(x)$ anomalies have an experimental analog in Raman scattering spectra where a pronounced frequency increase and a considerable decrease in the linewidth of the E_{2g} phonon mode at $x\approx 0.3$ was observed.[13,56] The fluctuating T_c values of the thin films from 11 to 14 K between $x=0.39$ and 0.47 might be interpreted as the formation of a T_c plateau that reminds of the 60 K plateau in the $T_c(\delta)$ dependence of the high-temperature superconductor $YBa_2Cu_3O_{7-\delta}$ between $\delta=0.3$ and 0.4.[57] The appearance of this plateau was ascribed to the formation of the ordered oxygen ortho II superstructure. In Ref. 55 the existence of a superstructure for $x=0.5$ with the optimum composition $MgAlB_4$ was reported and specified by alternating ordered Al and Mg triangular layers separated by the hexagonal B layers along the crystallographic c axis. This simple picture was later modified by the observation of an additional in-plane repeat period of about 10 nm.[58] Considering these findings the intimated emergence of a T_c plateau in Fig. 4(a) might be due to the superstructure $MgAlB_4$. Since the peculiarity extends over a wide average x range with considerable T_c fluctuations and broad transitions, the respective thin films are multiphase with an admixture of $MgAlB_4$ domains that seem to shield volume fractions with lower T_c so that T_c does not further decrease with progressive x. Finally, the reported T_c values of the $MgAlB_4$ phase differ enormously from nonsuperconducting[18,59] via 3 K[22] and 5 K[53] to 12 K.[55] Hence, it would be worth investigating the superstructure in more detail.

B. π energy gap of $Mg_{1-x}Al_xB_2$ thin films versus T_c

The measurement of the dI/dV versus V characteristic with the base- and the counter-electrode of the junction in the superconducting state (SIS′ configuration) is the most direct method of determining the value of the energy gap of S. Such a measurement at $T=1.2$ K in zero magnetic field is shown in Fig. 5 for three junctions A, B and C with an Al

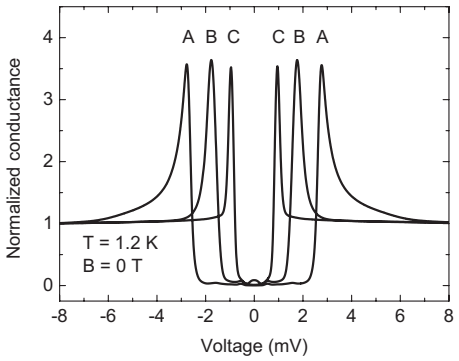

FIG. 5. Voltage dependence of the normalized conductance of three $Mg_{1-x}Al_xB_2$/insulator/In junctions with $x=0.16$ (junction A), 0.38 (junction B), and 0.49 (junction C) measured at 1.2 K in zero magnetic field with a rms modulation voltage ΔV of 32 μV. Both electrodes are superconducting. The conductance is normalized to the constant value of each junction with normal electrodes. The gap Δ_π of the diboride films can be directly determined from the position of the conductance peaks. The modulation voltage broadening of 1.7 ΔV can be neglected compared with the width of the conductance peaks.

concentration $x=0.16$, 0.38, and 0.49, respectively, of the $Mg_{1-x}Al_xB_2$ base electrode and In as a counterelectrode. The differential conductance is normalized to the conductance of the junctions with normalconducting electrodes which is constant in the small voltage range under consideration. It is noticeable that only one energy gap, obviously the small π energy gap, of the two-gap superconductor $Mg_{1-x}Al_xB_2$ ($x<0.5$) appears. Indications of the large σ energy gap could be observed in none of the 70 junctions investigated in this study. This finding is similar to that for the undoped MgB_2 in Ref. 40, where only in 2 of 50 junctions traces of the large gap were found. In principle, our observations can be explained by calculations of Dolgov *et al.*[60] for directional tunneling into MgB_2: One should observe the tunneling density of states of the π sheet, i.e., the small gap, with only negligible contribution from the large gap on the σ sheet for tunneling in the crystallographic c-axis direction. Our diboride films, however, are not epitaxial with the c-axis perpendicular to the substrate surface due to the low deposition temperature. At best they are c-axis textured with a broad mosaic spread. For tunneling directions different from the c-axis direction the large gap should show up more or less in the conductance characteristic. Another, more severe, restriction on the possible observation of directional tunneling was pointed out in a theoretical work by Walker:[61] Even if the roughness of the two interfaces base electrode/insulator and counter electrode/insulator is only a few atomic layers, the directionality of the tunnel current gets lost. We believe that the respective interfaces in our junctions are not flat enough for directional tunneling because the involved metal films are not epitaxial and the insulating layer in between them is polycrystalline and highly disordered or even amorphous. Hence, the question is still open, why only the small gap is observed in our type of layered junctions.

The values of the π energy gap Δ_π in dependence on the Al concentration x are easily determined by the voltage dis-

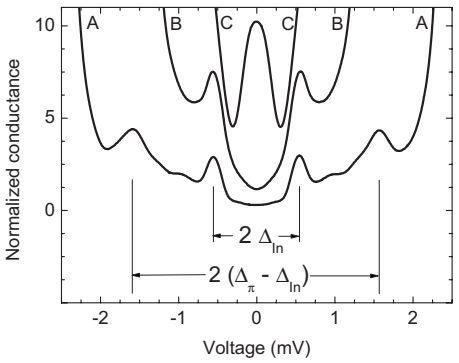

FIG. 6. Enlargement of Fig. 5 by a factor of 10 between −2 and 2 mV. The inner-gap features of the junctions are clearly resolved and discussed in the text. For a better differentiation between curve B and C, curve C was slightly shifted upwards.

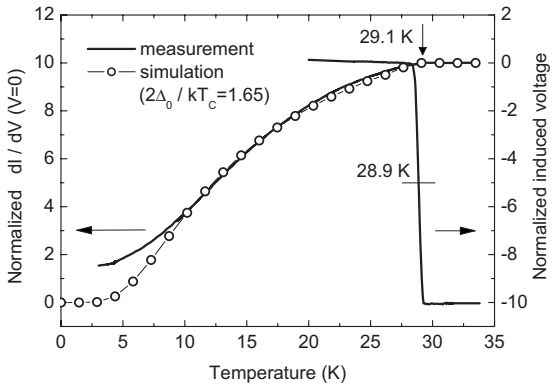

FIG. 7. Differential conductance dI/dV at zero bias, $V=0$, of a $Mg_{0.88}Al_{0.12}B_2$/insulator/In junction versus temperature. The conductance is normalized to the constant value of the junction with both electrodes in the normal state (straight line, left scale). The open circles are the result of a simulation with $2\Delta_0/kT_C=1.65$ as a fit parameter. The local gap T_c measured on the junction area of $\approx 10^{-3}$ cm^2 is 29.1 K. The nonlocal T_c of 28.9 K on a film area of ≈ 1 cm^2 is measured by the inductive transition curve (right scale). The good T_c agreement is another manifestation of the film homogeneity.

tance of the conductance peaks[62,63] which is $2(\Delta_\pi+\Delta_{In})/e$ (e: elementary charge). With $\Delta_{In}=0.54$ meV (Ref. 63) Δ_π close to 0 K for junctions A, B, and C in Fig. 5 amounts to 2.17, 1.23, and 0.41 meV, respectively. The conductance peaks show a finite width at half maximum of 0.84, 0.57, and 0.31 mV for junctions A, B, and C, respectively. The most likely explanation is a corresponding variation of energy gaps in the grains of the diboride films due to, e.g., nonuniform strain induced by differential contractions of films and substrates upon cooling. Nevertheless, alternative explanations such as lifetime effects or gap anisotropy cannot be ruled out.[64]

A nearer view reveals small structures within the gap of the junctions in Fig. 5. Therefore, the gap region is enlarged by a factor of 10 in Fig. 6. The appearance of the outer local maxima with a distance of $2(\Delta_\pi-\Delta_{In})$ in trace A corresponds to the well known logarithmic singularity at the gap difference in the *I-V* characteristic of SIS′ junctions.[65] Another remarkable feature are the two peaks in traces A and B with the distance $2\Delta_{In}$. Above the In gap until about ±1 mV, the characteristics are similar to those of In/insulator/normalconductor junctions.[66] This additional tunnel conductance is therefore interpreted as being due to tunneling into a small amount (about 1.6% in case A and 5.8% in case B) of normalconducting grains present at the diboride film surface. Below the In gap, the leakage conductance in the highly insulating junctions A and B only amounts to 0.3 and 1.1%, respectively, of the conductance with normal electrodes. Junction C exhibits a pronounced conductance peak at zero bias. Such an anomaly might have several origins. Since the junction resistance was only a few ohms, the peak could simply be due to a Josephson current. A zero bias conductance maximum is also typical for Andreev reflections[67] at a normalconductor-superconductor interface that is present in our proximity junctions. Finally, Rowell's discussion[44] of the conductance peak zero-bias anomaly, which typically occurs in junctions with proximity effect,[41] is based on Appelbaum's theory[68] of spin-flip scattering by magnetic impurities in the tunnel barrier.

Since the energy gap is temperature dependent and closes at T_c, the measurement of the conductance of the junction, e.g., at zero bias, in dependence on temperature offers the opportunity of determining T_c of the diboride film locally on the small junction area. We call the T_c determined this way "gap T_c" in distinction to the inductively measured nonlocal T_c (see Fig. 2) that is measured on an approximately 10^3 times larger area. Such a gap T_c measurement is shown in Fig. 7 (left scale) for a $Mg_{0.88}Al_{0.12}B_2$/insulator/In junction between 3 and 33 K. The differential conductance dI/dV at zero bias, $V=0$, is normalized to the constant conductance of the junction with normalconducting electrodes. The conductance is monotonic increasing with temperature up to a more or less pronounced kink, in this case at 29.1 K, which is the gap T_c of the diboride baseelectrode. The open circles are the result of a simulation of the measured gap T_c curve using the tables calculated by Bermon.[69] Excepting the range under 10 K, the best fit with minor deviations below 2% was obtained for the relation $2\Delta_0/kT_C=1.65$ (k: Boltzmann constant). This π gap derived value of the two-gap superconductor is significantly smaller than the Bardeen-Cooper-Schrieffer (BCS)-value of 3.52 in the weak-coupling limit. To compare local and nonlocal T_c, the inductively measured transition to superconductivity of the $Mg_{0.88}Al_{0.12}B_2$ film is also shown in Fig. 7 (right scale). The midpoint amounts to 28.9 K with a transition width of 0.5 K in good agreement with the gap T_c of 29.1 K. In general, the agreement was within ±1.5 K, which is another expression of the homogeneity of our Al doped diboride films.

The dependence of the π energy gap Δ_π at $T=1.2$ K on the gap T_c of the $Mg_{1-x}Al_xB_2$ thin films is exhibited in Fig. 8 for $x=0$ to $x=0.49$, i.e., for T_c values from 32 K to 3.2 K. At first glance, Δ_π decreases nearly linearly with decreasing T_c following the relation $\Delta_\pi=0.9\ kT_C$, ergo $2\Delta_\pi/kT_C=1.8$. This small value is comparable to that found for the simulation of the gap T_c curve in Fig. 7. It seems to be incompatible with the BCS-predictions of 3.52 and around 4 for the weak and strong-coupling limit, respectively. However, much smaller values are not unusual in the two-band extension of

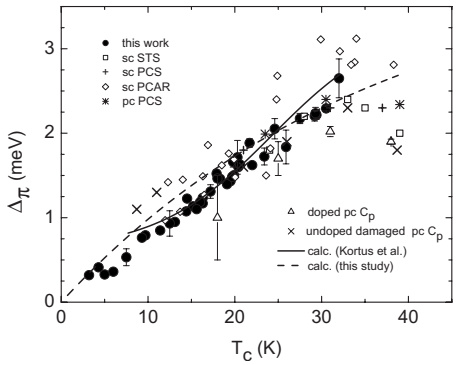

FIG. 8. Δ_π close to zero temperature versus T_c of diverse $Mg_{1-x}Al_xB_2$ samples; ●, this work (thin films, SIS′ junctions at 1.2 K); □, Ref. 27 (sc: single crystals, STS: scanning tunneling spectroscopy); +, Ref. 24 (PCS: point contact spectroscopy); ◇, Ref. 26 (PCAR: point-contact Andreev-reflection); ∗, Ref. 25 (pc: polycrystals); △, Ref. 14 (C_p: specific heat measurements); ×, Ref. 28; –, Ref. 19 (band filling calculation); --, this study (band filling calculation). Vertical bars on full circles indicate the statistical error of Δ_π upon gap measurements on different junctions with the same T_c of the $Mg_{1-x}Al_xB_2$ base electrode.

the BCS-theory[70] depending on the averaged interaction energies and the density of states in the two bands near the Fermi level. The monotonic-decreasing π gap with increasing Al doping can simply be explained by the band-filling model.[15–17,19] Two calculations based on this model are shown in Fig. 8 by the straight[19] and dashed lines. Interband scattering by impurities, that is predicted to increase the π gap, does not seem to play a role in our thin films. Data points from other groups determined on poly and single crystals by thermodynamic and various spectroscopic methods are also plotted in the figure and illustrate the wide spread of Δ_π-T_c dependencies already mentioned in the introduction. The linear decrease with decreasing T_c as well as the comparison of our Δ_π (T_c) data with the Δ_σ (T_c) data published in Refs. 14, 24–26, and 28 imply that our Δ_π values do not coincide with Δ_σ at any T_c. Therefore, the claim of the observation of gap merging at 11 K in Ref. 28 cannot be supported by this study.

C. Evolution of the Eliashberg function with Al doping

The quantity of central interest for electron-phonon-mediated superconductivity is the energy-dependent Eliashberg function $\alpha^2F(\omega)$, shortly α^2F, which is the phonon density of states weighted by the electron-phonon coupling strength averaged over directions in the reciprocal space. α^2F describes the scattering of quasiparticles on the Fermi surface via emission and absorption of virtual phonons. Electron tunneling spectroscopy,[35] as used in our studies, is the most powerful method to determine α^2F. In the differential conductance of SIN tunnel junctions, i.e., the quasiparticle density of states of the superconductor, phonon-induced structures are observed well above the energy gap and used to calculate α^2F via the single-band Eliashberg equations.

Figure 9(a) shows the differential conductance dI/dV of a $Mg_{0.89}Al_{0.11}B_2$/Al-oxide/In tunnel junction measured at 4.2 K ($Mg_{0.89}Al_{0.11}B_2$ superconducting, bold line) and 30 K (thin line) just above the T_c of the diboride superconductor. Only the conductance for negative bias of the In counterelectrode is shown which increases very slowly with increasing voltage (see Fig. 3) and is therefore best suited for tunneling spectroscopy. The phonon-induced features are clearly visible in the bold line although they only correspond to tiny relative conductance changes of a few 10^{-4}. The thin line in Fig. 9(a) represents the normal background (both electrodes normalconducting) which the phonon-induced structures are superposed on. It increases toward high voltage due to the voltage dependence of the tunneling matrix element and due to inelastic tunneling, as already mentioned above. In the evaluation of the conductance data, the effects of temperature smearing and of the superconducting state on the inelastic tunneling features have been taken into account following the procedure comprehensively described in Ref. 71. In the case of the undoped and Al-doped MgB_2, however, the corrections turned out to be of minor importance, because the strength of the inelastic tunneling features below 120 meV was at least ten times weaker than that of the phonon-induced features in the superconducting state. In order to demonstrate the phonon-induced structures more vividly, the measured negative derivative of the differential conductance, $-d^2I/dV^2$, is exhibited in Fig. 9(b) after subtraction of the normal-state background. In this presentation, the upward peaks correspond to peaks or shoulders in α^2F. The trace is dominated by three main peaks at 39, 59, and 90 mV comparable to the peaks at 39, 58, and 87 mV in Fig. 2(b) of Ref. 40 for undoped MgB_2. They reflect the coupling of electrons to the acoustic, lower-energy and higher-energy optical phonons, respectively. However, even moderate doping with 11% Al induces a slight shift of the main peaks to higher

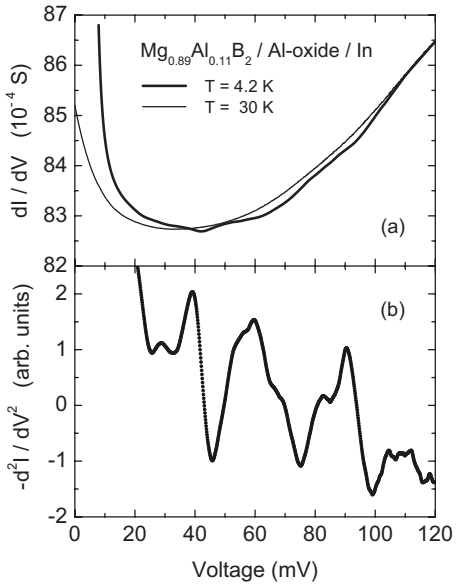

FIG. 9. (a) Differential conductance dI/dV versus bias voltage of a $Mg_{0.89}Al_{0.11}B_2$/Al-oxide/In tunnel junction measured at 4.2 K ($Mg_{0.89}Al_{0.11}B_2$ superconducting, In normalconducting; bold line) and at 30 K (both films normalconducting, thin line). (b) Negative second derivative of the *I-V* characteristic versus voltage measured at 4.2 K. The normal-state background has been subtracted.

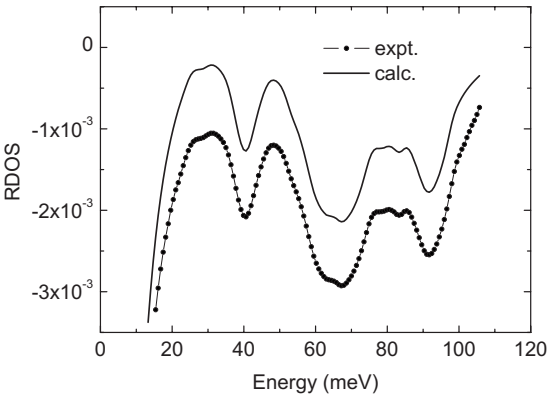

FIG. 10. Reduced density of states (RDOS) versus energy measured on a $Mg_{0.89}Al_{0.11}B_2$/Al-oxide/In junction (dashed-dotted line). The straight line is the result of a calculation using the PMMR-program with parameters $d/l=0.4$ and $R=0.002$ meV^{-1}.

energy and a substructure consisting of side peaks and shoulders at 29, 57, 67, and 83 mV.

The energy-dependent reduced density of states or RDOS as derived from the conductance data in Fig. 9 and the π energy gap measurements in Fig. 8 is shown in Fig. 10. It is defined as the relative deviation of the tunneling density of states from the BCS density of states. In our case, due to the small π gap and the high energy of the involved phonons, the deviation is very small and ranges from 1 to 3×10^{-3} on the energy scale up to 100 meV. As already mentioned in Sec. II, the RDOS is depressed below zero due to the proximity effect in our junctions, particularly at energies in the gap region below 20 meV. As predicted by Dolgov *et al.*[60] and experimentally evidenced by Geerk *et al.*[40] for pure MgB_2, the reduced density of states can be inverted to a so-called effective Eliashberg function of the Fermi surface π sheet using the single-band Eliashberg equations. With the RDOS as an input, the inversion procedure was performed using the McMillan-Rowell computer code including corrections for the proximity effect (PMMR). The best fit (straight line in Fig. 10) to the experimental data (dashed-dotted line) by using the PMMR inversion program was obtained with proximity parameters $d/l=0.4$ and $R=0.002$ meV^{-1}. The fit correctly reproduces the functional form of the measured RDOS, however, no proper set of fit parameters could be found to cancel out the small upward shift of the fit curve. We assume that this minor discrepancy has its origin in a tiny systematic error in the measurement of the conductance in the normal, i.e., resistive state of the films caused by the lack of a perfect four-terminal connection to the junction. This fundamental problem is well known and discussed in Ref. 35. The value of $R=0.002$ meV^{-1} can be used to roughly estimate the thickness d of the normalconducting proximity layer between the insulating tunnel barrier and the superconducting film. Assuming the proximity layer is Al, with $v_F^*\approx1.4\times10^8$ cm/s from Ref. 46, $R=0.002$ meV^{-1} corresponds to $d\approx0.9$ nm. This small value confirms our conjecture in section II that the proximity layer might be ultrathin. With $d/l=0.4$ and $d\approx0.9$ nm the effective scattering length l roughly results in 2.2 nm.

In our calculations, the $Mg_{1-x}Al_xB_2$ solid solution was modeled in the self-consistent virtual-crystal approximation

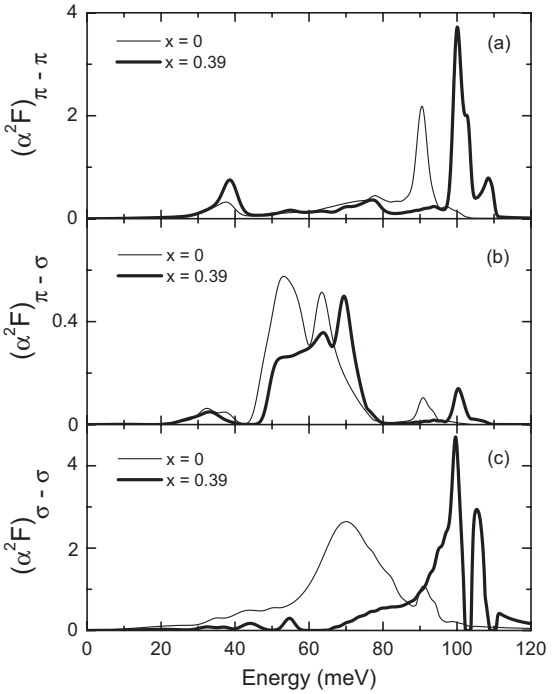

FIG. 11. (a) to (c) Eliashberg functions $(\alpha^2F)_{\pi-\pi}$, $(\alpha^2F)_{\pi-\sigma}$, and $(\alpha^2F)_{\sigma-\sigma}$, respectively, of the two-band superconductor $Mg_{1-x}Al_xB_2$ for $x=0$ (thin lines) and $x=0.39$ (thick lines) determined by first principles calculations in the generalized gradient approximation (GGA).

(VCA),[18] which was implemented within the mixed-basis pseudopotential (MBPP) method[72–74] by generating new pseudopotentials with a fractional nuclear charge at the Mg site for each x (atomic number $Z=12+x$) and by adjusting the valence charge accordingly.[18] The study was carried out with the generalized gradient approximation (GGA) applying the Perdew-Burke-Ernzerhof (PBE) version of the exchange-correlation functional.[75–77] The screened electron-phonon matrix elements were calculated via density functional perturbation theory[78,79] as implemented in the MBPP code,[74] which are the key elements of the Eliashberg theory.[80–83] The Eliashberg functions for all the band combinations were obtained by standard Fourier interpolation of quantities calculated with a very dense $36\times36\times36$ k-point mesh and a $6\times6\times6$ q-point mesh. The original four-band Eliashberg functions are projected onto an effective two-band model by averaging over the two σ and the two π bands, respectively. The RDOS of the π sheets were calculated in dependence on x by the solution of the two-band Eliashberg equations using the individual Eliashberg functions $(\alpha^2F)_{\pi-\pi}$, $(\alpha^2F)_{\pi-\sigma}$, and $(\alpha^2F)_{\sigma-\sigma}$ shown in Figs. 11(a)–11(c) for Al doping levels $x=0$ (thin lines) and $x=0.39$ (thick lines). The RDOS requires the gap function on the real axis, which is obtained by an iterative analytic continuation.[84] The theoretical RDOS were processed in the same way as the experimental ones, namely, inverted to effective Eliashberg functions $(\alpha^2F)_{\text{eff}}^{\text{th}}$ by the solution of the single-band Eliashberg equations using the standard MMR-computer code. The results for $x=0$, 0.11, 0.31, and 0.39 are shown in Figs. 12(a)–12(d), respectively, by the open circles. The theoretical effective Eliashberg

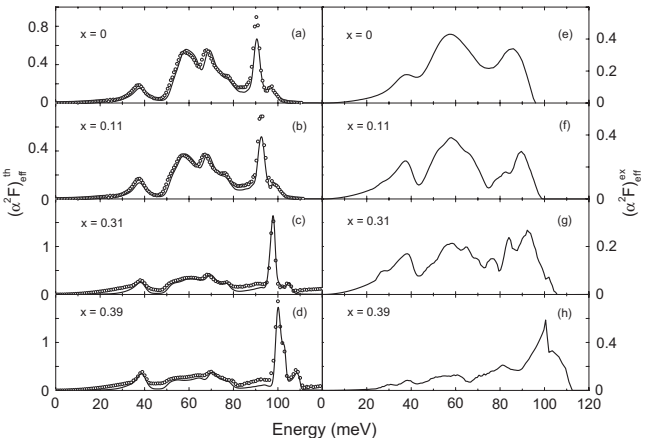

FIG. 12. (a) to (d) $(\alpha^2F)^{th}_{eff}$ of $Mg_{1-x}Al_xB_2$ for $x=0$, 0.11, 0.31, and 0.39, respectively, as determined by the inversion of the calculated RDOS of the π sheet using the single-band Eliashberg equations (open circles). The solid lines are the result of a superposition of $(\alpha^2F)_{\pi-\pi}$ and $(\alpha^2F)_{\pi-\sigma}$ (e) to (h) $(\alpha^2F)^{ex}_{eff}$ of $Mg_{1-x}Al_xB_2$ for $x=0$, 0.11, 0.31, and 0.39, respectively, as determined by the tunneling experiment.

functions with x as a parameter can be well reproduced by the solid lines in Figs. 12(a)–12(d), which represent a superposition of the intraband Eliashberg function $(\alpha^2F)_{\pi-\pi}\times N_\pi$ (N_π: electronic density of states of the π sheet at the Fermi energy) and the interband Eliashberg function $(\alpha^2F)_{\pi-\sigma}\times N_\sigma$ (N_σ: electronic density of states of the σ sheet at the Fermi energy) normalized to $N_\pi+3\times N_\sigma$. $(\alpha^2F)_{\pi-\sigma}$ was additionally weighted with the large ratio of Δ_σ and Δ_π of approximately three and shifted to higher energy by the difference $\Delta_\sigma-\Delta_\pi$ of approximately $2\Delta_\pi$.[40] The weighting factor Δ_σ/Δ_π remained the same with increasing Al doping level, since the ratio of the two gaps was not affected by doping, whereas the densities of states N_π and N_σ decreased with increasing x. The energy shift also decreased with increasing x due to the decreasing small energy gap (see Fig. 8). In the superposition, there was no contribution of the second intraband Eliashberg function $(\alpha^2F)_{\sigma-\sigma}$.

The experimental counterparts $(\alpha^2F)^{ex}_{eff}$ for Al doping levels $x=0$, 0.11, 0.31, and 0.39 are presented in Figs. 12(e)–12(h). The comparison with their calculated equivalents reveals a fair agreement between experiment and theory. The effective experimental $(\alpha^2F)^{ex}_{eff}$ for $x=0$ [Fig. 12(e)] was already discussed in detail in Ref. 40. Briefly, it comprises three broad peaks at 38, 58, and 86 meV. The two peaks at the low and high-energy end of the spectrum describe the coupling to the acoustic and high-energy optical phonons. The dominating central peak, that unusually has no counterpart in the phonon density of states, was identified as due to the $\pi-\sigma$ interband pairing interaction that is mainly responsible for the superconductivity of the π sheet. In the interband pairing interaction, low-energy optical phonons with vibrations of the B atoms perpendicular to the B planes are predominantly involved. The effective Eliashberg function evolves with increasing Al doping as follows: The overall three-peak configuration is roughly preserved. The low-energy peak at around 38 meV, which provides little contribution to the electron-phonon coupling, does not strongly react to the substitution of Mg by Al. However, the shape, spectral weight, and position of the dominating central peak at around 58 meV, that contributes the most to the effective electron-phonon coupling due to the strong interband pairing interaction, progressively change with increasing doping. In particular, the calculated partial coupling constant $\lambda_{\pi-\sigma}$ is reduced from 0.14 for $x=0$ to 0.07 for $x=0.39$ [see Fig. 11(b)]. The shift to higher energy and the reduced spectral weight with increasing x result in the reduced coupling constant and, hence, in a weakening of the interband pairing interaction, where both the σ and the π sheet of the Fermi surface are involved. Thus, the weakening of superconductivity of the π sheet directly reflects the changes in the electronic structure due to Al doping. As already pointed out in the introduction, they are characterized by the reduction of the densities of states N_π and N_σ and topological modifications of the Fermi surface σ sheet with its final disappearance, which both deeply affect the interband pairing interaction. Moreover, the distinct alterations observed in the position, shape, and spectral weight of our calculated intraband Eliashberg function $(\alpha^2F)_{\sigma-\sigma}$ in Fig. 11(c), where the partial coupling constant $\lambda_{\sigma-\sigma}$ was reduced from 0.85 for $x=0$ to 0.28 for $x=0.39$, are also a clear manifestation of the changes in the electronic band structure with increasing Al doping. Drastic changes of the shape, position and spectral weight also concern the peak at the high-energy end. It is continuously shifted to higher energy, namely, from 86 meV for $x=0$ in Fig. 12(e) to 101 meV for $x=0.39$ in Fig. 12(h). For the latter Al concentration, the peak has become the strongest one in the entire spectrum. It is worth mentioning that our observations at the low and high-energy end of the effective α^2F in dependence on x were also made in the generalized phonon density of states of bulk samples measured with inelastic neutron scattering.[56] To complete the discussion of Fig. 12, the effective coupling constant λ^{ex}_{eff} and the Coulomb pseudopotential μ^* (expt.) determined from $(\alpha^2F)^{ex}_{eff}$ decreased continuously from 0.65 and 0.10 for $x=0$ to 0.38 and 0.05 for $x=0.39$, respectively. The calculated quantities λ^{th}_{eff} and μ^* (theor.) derived from $(\alpha^2F)^{th}_{eff}$ were slightly lower with relative deviations not larger than 10%.

IV. SUMMARY AND CONCLUSION

We have prepared *in situ* superconducting $Mg_{1-x}Al_xB_2$ thin films ($0\leq x<0.5$) by sublimation of Mg and cosputtering of B and Al. The dependence of the critical temperature T_c on the Al concentration x was studied. In addition to a linear decrease with a slope of −0.4 K per at% Al, that can be explained by the assumption of band filling with extra electrons, a sharp drop and the formation of a plateaulike feature were observed. These anomalies might result from a topological change of the Fermi surface σ sheet predicted by band-structure calculations and the growth of domains of the superstructure $MgAlB_4$ with a T_c around 12 K, respectively.

Planar tunnel junctions on the $Mg_{1-x}Al_xB_2$ thin films revealed the proximity effect caused by a presumably ultrathin normalconducting layer, likely of Al, between superconductor and tunnel barrier. The quality of the barrier with

respect to thickness and height significantly improved by the employment of the aluminum overlayer technique, i.e., the growth of artificial aluminum oxide on the superconducting film. Only the energy gap on the π sheet of the Fermi surface was observed which means that exclusively superconductivity of the π sheet is sampled in our type of junctions. The π energy gap as measured in the SIS′ configuration of the junctions decreased approximately linearly with decreasing T_c with a slope of 0.9 k (k: Boltzmann constant). The decrease is in agreement with the model of band filling, whereas interband scattering by the Al impurities does not seem to play any role in the films. Though the σ energy gap was not observed in the thin film experiments, the results for the π energy gap were highly consistent with others published for bulk forms of the material, such as poly and single crystals, in spite of the interaction of the thin film with the substrate that could induce additional interface effects such as pseudomorphic growth, strain and dislocations.

The progressive loss of superconductivity with increasing Al doping was reflected in both the calculations and the experiment by characteristic modifications in the effective Eliashberg function α^2F of the π sheet compared to undoped MgB_2: The dominating central peak, which is due to the $\pi-\sigma$ interband pairing interaction and contributes most to superconductivity on the π sheet, is progressively weakened and shifted to higher energy resulting in a reduction of 50% of the coupling constant $\lambda_{\pi-\sigma}$. This effect is correlated with the reduction of the electronic density of states and the topological change of the Fermi surface predicted by band-structure calculations. The observed renormalization of the peak at the high-energy end is in accordance with measurements of the phonon density of states using inelastic neutron scattering.

ACKNOWLEDGMENTS

The authors would like to thank A. Beck and E.-P. Knaetsch for technical assistance. Work at Cinvestav was supported by the Consejo Nacional de Ciencia y Tecnología (CONACYT-México) under Grant No. 43830-F. One of the authors (O.P.-S.) gratefully acknowledges financial support from CONACYT-México and Deutscher Akademischer Austauschdienst (DAAD).

*Corresponding author; rudolf.schneider2@kit.edu

[1] M. Jones and R. Marsh, J. Am. Chem. Soc. **76**, 1434 (1954).
[2] J. Nagamatsu, N. Nakagawa, T. Muranaka, Y. Zenitari, and J. Akimitsu, Nature (London) **410**, 63 (2001).
[3] T. Oguchi, J. Phys. Soc. Jpn. **71**, 1495 (2002).
[4] M. Mudgel, V. P. S. Awana, H. Kishan, I. Felner, G. A. Alvarez, and G. L. Bhalla, J. Appl. Phys. **105**, 07E313 (2009).
[5] Y. Kamihara, T. Watanabe, M. Hirano, and H. Hosono, J. Am. Chem. Soc. **130**, 3296 (2008).
[6] M. V. Sadovskii, Phys. Usp. **51**, 1201 (2008).
[7] B. W. Roberts, J. Phys. Chem. Ref. Data **5**, 581 (1976).
[8] J. G. Bednorz and K. A. Müller, Z. Phys. B **64**, 189 (1986).
[9] M. Rotter, M. Pangerl, M. Tegel, and D. Johrendt, Angew. Chem. Int. Ed. **47**, 7949 (2008).
[10] S. Lee, Physica C **456**, 14 (2007).
[11] J. S. Slusky, N. Rogado, K. A. Regan, M. A. Hayward, P. Khalifah, T. He, K. Inumaru, S. M. Loureiro, M. K. Haas, H. W. Zandbergen, and R. J. Cava, Nature (London) **410**, 343 (2001).
[12] J. Karpinski, N. D. Zhigadlo, G. Schuck, S. M. Kazakov, B. Batlogg, K. Rogacki, R. Puzniak, J. Jun, E. Müller, P. Wägli, R. Gonnelli, D. Daghero, G. A. Ummarino, and V. A. Stepanov, Phys. Rev. B **71**, 174506 (2005).
[13] P. Postorino, A. Congeduti, P. Dore, A. Nucara, A. Bianconi, D. Di Castro, S. De Negri, and A. Saccone, Phys. Rev. B **65**, 020507(R) (2001).
[14] M. Putti, M. Affronte, P. Manfrinetti, and A. Palenzona, Phys. Rev. B **68**, 094514 (2003).
[15] J. M. An and W. E. Pickett, Phys. Rev. Lett. **86**, 4366 (2001).
[16] J. Kortus, I. I. Mazin, K. D. Belashchenko, V. P. Antropov, and L. L. Boyer, Phys. Rev. Lett. **86**, 4656 (2001).
[17] O. de la Peña, A. Aguayo, and R. de Coss, Phys. Rev. B **66**, 012511 (2002).
[18] O. De la Peña-Seaman, R. de Coss, R. Heid, and K.-P. Bohnen, Phys. Rev. B **79**, 134523 (2009); (private communication).
[19] J. Kortus, O. V. Dolgov, R. K. Kremer, and A. A. Golubov, Phys. Rev. Lett. **94**, 027002 (2005).
[20] A. A. Golubov and I. I. Mazin, Phys. Rev. B **55**, 15146 (1997).
[21] I. I. Mazin, O. K. Andersen, O. Jepsen, O. V. Dolgov, J. Kortus, A. A. Golubov, A. B. Kuz'menko, and D. van der Marel, Phys. Rev. Lett. **89**, 107002 (2002).
[22] A. Bussmann-Holder and A. Bianconi, Phys. Rev. B **67**, 132509 (2003).
[23] S. C. Erwin and I. I. Mazin, Phys. Rev. B **68**, 132505 (2003).
[24] T. Klein, L. Lyard, J. Marcus, C. Marcenat, P. Szabó, Z. Hol'anová, P. Samuely, B. W. Kang, H.-J. Kim, H.-S. Lee, H.-K. Lee, and S.-I. Lee, Phys. Rev. B **73**, 224528 (2006).
[25] P. Szabó, P. Samuely, Z. Pribulová, M. Angst, S. Bud'ko, P. C. Canfield, and J. Marcus, Phys. Rev. B **75**, 144507 (2007).
[26] D. Daghero, D. Delaude, A. Calzolari, M. Tortello, G. A. Ummarino, R. S. Gonnelli, V. A. Stepanov, N. D. Zhigadlo, S. Katrych, and J. Karpinski, J. Phys.: Condens. Matter **20**, 085225 (2008).
[27] F. Giubileo, F. Bobba, A. Scarfato, A. M. Cucolo, A. Kohen, D. Roditchev, N. D. Zhigadlo, and J. Karpinski, Phys. Rev. B **76**, 024507 (2007).
[28] M. Putti, M. Affronte, C. Ferdeghini, P. Manfrinetti, C. Tarantini, and E. Lehmann, Phys. Rev. Lett. **96**, 077003 (2006).
[29] R. Di Capua, H. U. Aebersold, C. Ferdeghini, V. Ferrando, P. Orgiani, M. Putti, M. Salluzzo, R. Vaglio, and X. X. Xi, Phys. Rev. B **75**, 014515 (2007).
[30] M. Iavarone, R. Di Capua, A. E. Koshelev, W. K. Kwok, F. Chiarella, R. Vaglio, W. N. Kang, E. M. Choi, H. J. Kim, S. I. Lee, A. V. Pogrebnyakov, J. M. Redwing, and X. X. Xi, Phys. Rev. B **71**, 214502 (2005).
[31] M. Putti, C. Ferdeghini, M. Monni, I. Pallecchi, C. Tarantini, P. Manfrinetti, A. Palenzona, D. Daghero, R. S. Gonnelli, and V. A.

Stepanov, Phys. Rev. B **71**, 144505 (2005).
[32] L. D. Cooley, A. J. Zambano, A. R. Moodenbaugh, R. F. Klie, Jin-Cheng Zheng, and Yimei Zhu, Phys. Rev. Lett. **95**, 267002 (2005).
[33] J. Kortus, Physica C **456**, 54 (2007).
[34] I. Giaever, Phys. Rev. Lett. **5**, 147 (1960); **5**, 464 (1960).
[35] W. L. McMillan and J. M. Rowell, in *Superconductivity*, edited by R. D. Parks (Dekker, New York, 1969), Vol. 1, p. 561.
[36] R. Schneider, J. Geerk, F. Ratzel, G. Linker, and A. G. Zaitsev, Appl. Phys. Lett. **85**, 5290 (2004).
[37] R. Schneider, J. Geerk, G. Linker, F. Ratzel, A. G. Zaitsev, and B. Obst, Physica C **423**, 89 (2005).
[38] R. Schneider, J. Geerk, A. G. Zaitsev, and H. v. Löhneysen, Appl. Phys. Lett. **91**, 022509 (2007).
[39] W. K. Chu, J. W. Mayer, and M. A. Nicolet, *Backscattering Spectrometry* (Academic, New York, 1978).
[40] J. Geerk, R. Schneider, G. Linker, A. G. Zaitsev, R. Heid, K.-P. Bohnen, and H. v. Löhneysen, Phys. Rev. Lett. **94**, 227005 (2005).
[41] J. M. Rowell, M. Gurvitch, and J. Geerk, Phys. Rev. B **24**, 2278 (1981).
[42] W. F. Brinkman, R. C. Dynes, and J. M. Rowell, J. Appl. Phys. **41**, 1915 (1970).
[43] D. H. Douglass, Jr. and L. M. Falicov, in *Progress in Low Temperature Physics*, edited by C. J. Gorter (North-Holland, Amsterdam, 1964), Vol. 4, p. 97.
[44] J. M. Rowell, in *Tunneling Phenomena in Solids*, edited by E. Burstein and S. Lundqvist (Plenum, New York, 1969), p. 385.
[45] J. S. Moodera, R. Meservey, and P. M. Tedrow, Appl. Phys. Lett. **41**, 488 (1982).
[46] E. L. Wolf and G. B. Arnold, Phys. Rep. **91**, 31 (1982).
[47] U. Schneider, J. Geerk, and H. Rietschel, in *Proceedings of the 17th International Conference on Low Temperature Physics*, Karlsruhe, 1984, edited by U. Eckern, A. Schmid, W. Weber, and H. Wühl (Elsevier, New York, 1984), p. 489.
[48] E. L. Wolf, J. Zasadzinski, J. W. Osmun, and G. B. Arnold, J. Low Temp. Phys. **40**, 19 (1980).
[49] W. N. Hubin, University of Illinois Technical Report No. 182, 1970 (unpublished).
[50] E. L. Wolf and R. J. Noer, Solid State Commun. **30**, 391 (1979).
[51] B. L. Blackford, Rev. Sci. Instrum. **42**, 1198 (1971).
[52] J. G. Adler and J. E. Jackson, Rev. Sci. Instrum. **37**, 1049 (1966).
[53] A. Bianconi, S. Agrestini, D. Di Castro, G. Campi, G. Zangari, N. L. Saini, A. Saccone, S. De Negri, M. Giovannini, G. Profeta, A. Continenza, G. Satta, S. Massidda, A. Cassetta, A. Pifferi, and M. Colapietro, Phys. Rev. B **65**, 174515 (2002).
[54] R. S. Gonnelli, D. Daghero, G. A. Ummarino, M. Tortello, D. Delaude, V. A. Stepanov, and J. Karpinski, Physica C **456**, 134 (2007).
[55] J. Q. Li, L. Li, F. M. Liu, C. Dong, J. Y. Xiang, and Z. X. Zhao, Phys. Rev. B **65**, 132505 (2002).
[56] B. Renker, K.-P. Bohnen, R. Heid, D. Ernst, H. Schober, M. Koza, P. Adelmann, P. Schweiss, and T. Wolf, Phys. Rev. Lett. **88**, 067001 (2002).
[57] R. J. Cava, B. Batlogg, C. H. Chen, E. A. Rietman, S. M. Zahurak, and D. Werner, Nature (London) **329**, 423 (1987).
[58] H. W. Zandbergen, M. Y. Wu, H. Jiang, M. A. Hayward, M. K. Haas, and R. J. Cava, Physica C **366**, 221 (2002).
[59] J. Karpinski, N. D. Zhigadlo, S. Katrych, R. Puzniak, K. Rogacki, and R. Gonnelli, Physica C **456**, 3 (2007).
[60] O. V. Dolgov, R. S. Gonnelli, G. A. Ummarino, A. A. Golubov, S. V. Shulga, and J. Kortus, Phys. Rev. B **68**, 132503 (2003).
[61] M. B. Walker, Phys. Rev. B **60**, 9283 (1999).
[62] B. L. Blackford, J. Low Temp. Phys. **23**, 43 (1976).
[63] E. L. Wolf, *Principles of Electron Tunneling Spectroscopy* (Oxford University Press, London, 1985).
[64] S. Bermon and D. M. Ginsberg, Phys. Rev. **135**, A306 (1964).
[65] J. Nicol, S. Shapiro, and P. H. Smith, Phys. Rev. Lett. **5**, 461 (1960).
[66] J. Geerk, U. Kaufmann, W. Bangert, and H. Rietschel, Phys. Rev. B **33**, 1621 (1986).
[67] A. F. Andreev, Sov. Phys. JETP **19**, 1228 (1964).
[68] J. Appelbaum, Phys. Rev. Lett. **17**, 91 (1966).
[69] S. Bermon, University of Illinois Technical Report No. 1, 1964 (unpublished).
[70] H. Suhl, B. T. Matthias, and L. R. Walker, Phys. Rev. Lett. **3**, 552 (1959).
[71] J. Geerk and H. v. Löhneysen, Phys. Rev. Lett. **99**, 257005 (2007).
[72] S. G. Louie, K. M. Ho, and M. L. Cohen, Phys. Rev. B **19**, 1774 (1979).
[73] B. Meyer, C. Elsässer, and M. Fähnle, FORTRAN90, Program for Mixed-Basis Pseudopotential Calculations for Crystals, Max-Planck-Institut für Metallforschung, Stuttgart.
[74] R. Heid and K.-P. Bohnen, Phys. Rev. B **60**, R3709 (1999).
[75] V. Ozolins and M. Körling, Phys. Rev. B **48**, 18304 (1993).
[76] K. Kokko and M. P. Das, J. Phys.: Condens. Matter **10**, 1285 (1998).
[77] J. P. Perdew, K. Burke, and M. Ernzerhof, Phys. Rev. Lett. **77**, 3865 (1996).
[78] S. Baroni, P. Giannozzi, and A. Testa, Phys. Rev. Lett. **58**, 1861 (1987).
[79] P. Giannozzi, S. de Gironcoli, P. Pavone, and S. Baroni, Phys. Rev. B **43**, 7231 (1991).
[80] G. M. Eliashberg, Sov. Phys. JETP **11**, 696 (1960).
[81] J. P. Carbotte, Rev. Mod. Phys. **62**, 1027 (1990).
[82] F. Marsiglio and J. P. Carbotte, *The Physics of Superconductors* (Springer, Berlin, Heidelberg, 2003), Vol. 1, p. 231.
[83] S. Y. Savrasov, D. Y. Savrasov, and O. K. Andersen, Phys. Rev. Lett. **72**, 372 (1994).
[84] F. Marsiglio, M. Schossmann, and J. P. Carbotte, Phys. Rev. B **37**, 4965 (1988).